

Elucidation of rGO Incorporation on Structural, Morphological and Optical Properties of rGO/ZnO Nanocomposites for Flexible Humidity Sensor Applications

A. Shamsul Rahimi A. Subki

*Faculty of Electrical and Electronics Engineering Technology,
Universiti Teknikal Malaysia Melaka, Hang Tuah Jaya,
76100 Durian Tunggal, Melaka, Malaysia*

Mohamad Hafiz Mamat, Mohamad Rusop Mahmood
NANO-ElecTronic Centre (NET), School of Electrical Engineering,
College of Engineering, Universiti Teknologi MARA,
40450 Shah Alam, Selangor, Malaysia
mhmamai@uitm.edu.my

*Dayana Kamaruzaman
School of Electrical Engineering, College of Engineering,
Universiti Teknologi MARA, Cawangan Terengganu, Kampus Dungun,
23000 Dungun, Terengganu, Malaysia*

*Mohd Hanapiah Abdullah, Musa Mohamed Zahidi,
Center for Electrical Engineering Studies, Universiti Teknologi MARA,
Cawangan Pulau Pinang, 13500 Permatang Pauh, Pulau Pinang, Malaysia*

*N. Vasimalai, I.B. Shameem Banu
School of Physical and Chemical Sciences, B. S. Abdur Rahman Crescent
Institute of Science and Technology, Vandalur, Chennai, 600 048,
Tamil Nadu, India*

*Muhammad Danang Birowosuto
Łukasiewicz Research Network-PORT Polish Center for Technology
Development, Stabłowicka 147, 54-066 Wrocław, Poland*

ABSTRACT

The effect on structural, morphological and optical characteristics towards humidity sensing capability was elucidated as humidity-sensitive sensing material that is made by composting zinc oxide nanostructured powder (ZN) nanoparticles with varying capacities of reduced graphene oxide (rGO). The ZN was successfully synthesized through the ultrasonicated solution immersion technique and the rGO/ZN (rZN) nanocomposite sensing material was spread on cellulose substrates employing a simple brush printing technique. XRD, FESEM and UV-Vis Diffuse Reflectance Spectroscopy were utilized to examine the morphological and optical properties of the pristine ZN and rZN nanocomposites. As per the FESEM assessment, ZN nanoparticles with variable sizes were evenly distributed, adhered to, and irregularly positioned on filter paper cellulose fibres. The average reflectance in the visible region declined substantially as the rGO content increased. According to the estimated Urbach energy, the defects in the sensing materials increased as the rGO content increased. The humidity response capability of the nanocomposites exhibits a significant reliance on the quantity of rGO integrated, with the maximum humidity sensitivity achieved for the 1.0 wt.% rGO dosage. At a high operating temperature (85 °C), the humidity sensor based on rZN-1.0% nanocomposite exhibits an amplified humidity sensing response current value. These outcomes indicate that rZN nanocomposites have the potential to operate as a humidity-sensitive sensing material with great sensitivity.

Keywords: Zinc Oxide Nanoparticles; Reduced Graphene Oxide; Kubelka-Munk; Flexible Humidity Sensor

Introduction

Humidity sensors are tremendously significant since they are utilized in a diversity of applications for instance climate forecasting, healthcare industries, food industry sectors, semiconductor fabrication fields, and agriculture [1]–[3]. Better sensitivity, reliance on processing temperature, shortest response/recovery time, strong reproducibility, minimal hysteresis value, prolonged shelf life durability, capability to tolerate contaminants, and cheaper production rate can all be used to specify an excellent humidity sensor [4]. Metal oxide (MOx) semiconductors are one of the most commonly used materials in humidity sensors. The reason for this is the significant surface ratio, green materials, low cost, improved sensitivity, ease of production, rapid reaction with enhanced sensitivity, and excellent durability towards temperature and chemical fluctuation.

Zinc oxide (ZnO) has piqued the interest of scholars studying its possibilities as a humidity-sensitive material due to its accessible and modifiable structure, huge resistivity spectrum, and great chemical and thermal stability [5]. ZnO is a non-organic semiconductor compound with ionicity that occurs on the border between covalent and ionic semiconductors. In ambient conditions, ZnO possesses a vast and linear energy bandgap, comprising 60 meV of moderately substantial exciton potential [6]. Graphene has arisen as a favourable sensing material due to its high conductivity, charge mobility, and mechanical and chemical robustness. Among graphene derivatives, reduced graphene oxide (rGO) has attracted considerable interest in the implementation of sensor devices, owing to its highly conductive sp^2 carbon atom film, which functions as an anchor to encourage electron transfer in metal oxide nanoparticles, resulting in improved sensing performance, exquisite electrical and mechanical attributes [7].

Unfortunately, humidity sensors based on pristine ZnO have a variety of drawbacks, involving a shorter storage lifespan, lengthy response/recovery duration, minimal linearity, and frail hysteresis, which limit their potential purposes [8]. Recent progressions have displayed that the addition of graphene elements and derivatives with MOx nanostructures is a reliable approach for constructing highly efficient sensors due to their conceivably huge surface vicinity, outstanding mobility, elevated conductance, plentiful deficiency domains, and remarkably elevated thermal conductivity and mechanical strength [9]. Worth to mention, that using graphene (G, GO, or rGO) as a sole sensing material, on the other hand, results in insufficient sensing performance for changes in relative humidity (RH). As a result of combining two or more semiconductor materials with different energy gaps, which allowed for the recombination of electron-hole pairs, which simultaneously modified material characteristics, the main objective of enhancing the effectiveness and performance parameters of resistive-type humidity sensors constructed from ZnO-sensitive sensing material is achievable as proved by previous works [10]–[12].

In this paper, the effect of various rGO dosages on the structural, morphological and optical properties of pristine ZnO and rGO/ZnO nanocomposites on humidity sensing capabilities has been discussed. Albeit the properties of ZnO nanoparticles have been thoroughly explored in the literature, the impacts of rGO insertion into ZnO have been scarcely discussed in detail, particularly for humidity sensing applications. As a result, it is worthwhile to investigate the structural, morphological, optical and humidity sensing characteristics of rGO incorporation into pristine ZnO.

Methodology

To synthesize ZnO nanostructured powders (ZN), zinc nitrate hexahydrate [$\text{Zn}(\text{NO}_3)_2 \cdot 6\text{H}_2\text{O}$, 98.5%, Riendemann Schmidt] and hexamethylenetetramine ($\text{C}_6\text{H}_{12}\text{N}_4$, 99% purity, Aldrich) were analytical grades. The pristine ZN was synthesized through the ultrasonicated solution immersion route by dissolving the equimolar concentration of $\text{Zn}(\text{NO}_3)_2 \cdot 6\text{H}_2\text{O}$ and $\text{C}_6\text{H}_{12}\text{N}_4$ in a beaker filled with deionized (DI) water, followed by the sonicated procedure for 30 min in an ultrasonic bath (Hwashin Technology). Afterwards, the homogeneity solution was poured into a Schott bottle (DURAN) and immersed in a water bath (Memmert) for 4 hours at 95 °C. Following the immersion procedure, the precipitates formed were collected and dried (40 °C, 24 hours). The dehydrated sample was annealed in an ambient environment for 1 hour at 500 °C in a chamber furnace (Protherm).

Before the deposition of sensitive sensing material, the nanocomposite of sensitive sensing material was first prepared. The standard procedures have been discussed elsewhere [13]. Later, the synthesized ZN (1 g) and rGO powder (1 mg) purchased from Suzhou Hengqiu were dispersed in a 5 ml binder agent (Clear glue, UMOE) and stirred to obtain a homogeneous solution. The formed paste-like nanocomposite slurry sensing material mixture was marked as rZN-0.1%. An analogous process was used to produce nanocomposites with various rGO powder compositions and corresponding samples were labelled as rZN-0.5%, rZN-1.0%, rZN-1.5%, and rZN-2.0%, respectively. To perform morphological, optical and humidity sensing performance characterization, cellulose-based paper (Whatman) was used as a substrate. Using the brush printing process, a sensing material (rZN-0.1%) homogeneous paste-like nanocomposite slurry was successively brushed on a cellulose substrate to construct the sensing membrane. The deposited paste was then cured at ambience condition for 15 min followed by the functioning electrode patterned over the sensing membrane. The crystal structure and peak identification were epitomized via multipurpose X-ray diffractometer analysis (XRD; PANalytical X'Pert Pro MRD). The morphological studies analysis for the PZN and rGO/ZN nanocomposite films were accomplished utilizing field emission scanning electron microscopy (FESEM; Hitachi SU-8030) while, the optical reflectance measurements, in the ultra-violet visible (UV-vis) range, were carried out using dual-beam ultraviolet, visible light and near-infrared, diffuse reflectance spectroscopy (DRS; Varian Cary 5000). The humidity response plot and data were obtained via electrical measurements using ESPEC-SH261 humidity and temperature chamber with Keithley 2400 Source Meter unit.

Result and Discussion

X-ray diffraction (XRD) assessment was employed to assess the crystal structure and peak identification attributes of the as-produced PZN and rZN nanocomposites and further validate the formation of the nanocomposite. Figure 1 depicts the XRD profiles of PZN, and rZN nanocomposites with varying rGO dosages. The XRD profile of PZN and all rZN samples exhibits an inheritance of diffraction peaks that are associated with the ZnO wurtzite hexagonal configuration [14]. Furthermore, the diffraction peak, 2 values for three major peaks and five minor peaks are found at 31.92° , 34.59° , 36.39° , 47.69° , 56.74° , 63.02° , 68.08° , and 69.22° , which refer to the (100), (002), 101) (102), (110), (103), (112), and (201) planes, respectively [15]. The occurrence of numerous distinctive peak positions with significant intensities indicates that the as-produced ZN is polycrystalline and retains well crystalline structures. Lacking impurity-associated diffraction amplitudes, confirming the synthesis of a pristine phase of ZN. After the hybridization of ZN with rGO, the diffraction profiles of the rZN nanocomposites are identical to one another and comparable to PZN, suggesting that the crystal structure of the ZN crystal was unchanged, implying that rGO was surface bonded with ZN.

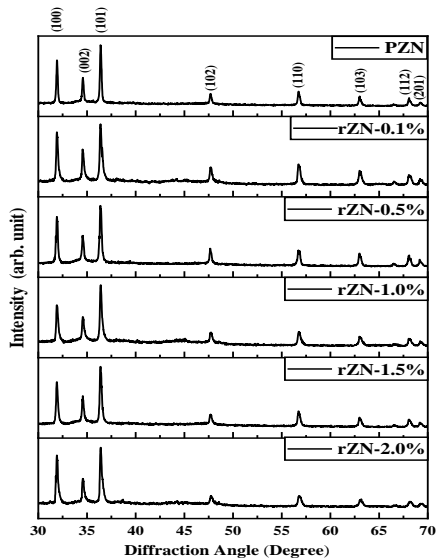


Figure 1: Diffraction profile of PZN and rZN nanocomposites at different rGO content

Using field emission scanning electron microscopy (FESEM), the surface morphological features of pristine ZN (PZN) and rGO/ZN (rZN) nanocomposites were examined, as well as the impact of rGO integration on the microscopic structure. Figure 2 portrays the morphology of PZN and rZN nanocomposites surface comprising 0.1 wt.%, 0.5 wt.%, 1.0 wt.%, 1.5, and 2.0 wt.% of rGO amount deposited on cellulose substrate at magnifications of $\times 20000$. The flattening surfaces of ZN nanoparticles vary in diameters and are identically distributed, affixed, and arbitrarily positioned onto the cellulose strands, as depicted in the micrograph in Figures 2a–f. Excitingly, raising the quantity of rGO dosage observably did not affect the morphology of ZN in rZN nanocomposites, but did marginally reduce the diameter of ZN nanoparticles. The mean diameter of consolidated ZN in rZN nanocomposites spans between 50 to 300 nm. Furthermore, the ZN nanoparticles are separated from their connected network and attached to the surface of rGO [16]. The rZN nanocomposite formation is validated by the binding of ZN nanoparticles to the rGO layers. Furthermore, the rGO sheet becomes denser and exemplify a tightly packed structure comprising ZN nanoparticles as the percentage of rGO content increase. As shown in Figures 2b–f, the surfaces and edges of the nanoparticles were less visible, verifying that the thin transparent rGO layers were wrapped and covered the ZN structure. These observations proved that the nanocomposite is created, comprising the rGO sheets and ZN nanoparticles.

Geometrical porosity and particularly large surface area are essential properties in rZN nanocomposites for enhancing humidity sensing capabilities. The integration of nano-granulated formed ZN nanoparticles with rGO layers was observed to potentially offer a sensing material with porosity structure and high specific surface area. As for rZN nanocomposites, the rGO is disseminated across the ZN to construct a networked arrangement. It is observable that folded rGO layers encapsulate nano-granulated ZN nanoparticles, which have a superior specific surface area and make outstanding contact with neighbouring nanoparticles. This interlinked multilayered structure accelerates the transfer of electrons between ZN and rGO, improving the sensing film's surface area and thereby improving humidity sensing sensitivity [17]. Moreover, the porosity detected throughout all rZN nanocomposites is anticipated to enable adsorption sites for incoming water molecules.

The optical properties of the pristine ZN (PZN) and rGO/ZN (rZN) nanocomposites are shown in Figure 3. In the UV region spectrum (< 400 nm), all of these samples exhibited intense light absorption, which is facilitated by electron transportation from the valence band to the conduction band. Compared to PZN, in the UV spectrum region, rZN nanocomposites indicate lower light absorption. The light absorption for rZN nanocomposite samples was significantly affected by the different amounts of rGO dosage. Therefore, as the amount of the rGO dosage increased, the intensity of visible

light absorption for rZn nanocomposites in the visible region (400–800 nm) was observed to increase significantly. This may be attributable to the relatively superior rGO absorption coefficient in the visible light spectrum and an improved surface electric charge related to oxides in the rZn nanocomposites, which are related to the electron-hole pairs formation process during light illumination [18]-[19]. The observed results were supported by previous reports [20]-[21].

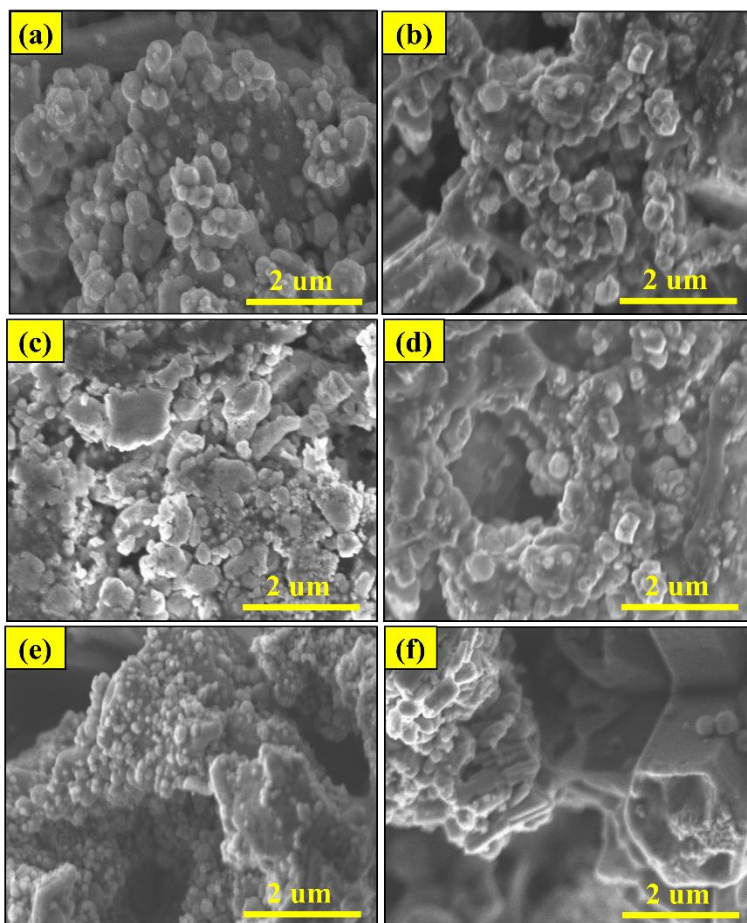


Figure 2: FESEM morphology ($\times 20000$ magnifications; applied voltage of 5 kV) of PZN and rGO/Zn nanocomposites at different amount of rGO deposited on cellulose substrate: (a) PZN, (b) 0.5 wt.%, (c) 1.0 wt.%, (d) 1.5 wt.% and (e) 2.0 wt.%

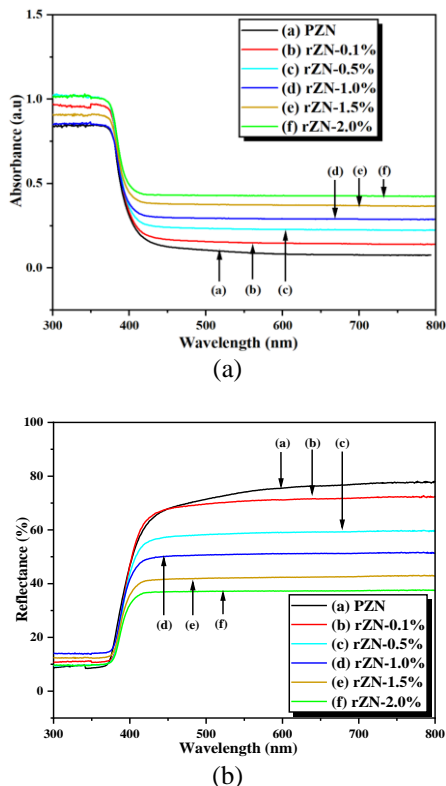


Figure 3: Ultraviolet-visible diffuse reflectance spectra (UV-Vis DRS) of PZN and rZN nanocomposites with a different weight percentage of rGO dosage; (a) the absorbance spectra, and (b) the reflectance spectra

Kubelka-Munk method was used to calculate and estimate the direct optical band gap energy with decent accuracy from weakly absorbing samples. Kubelka-Munk's theory is based on a simplified assessment of incoming light's interaction with a specimen. This theory holds that the materials were homogeneous, isotropic, non-fluorescent, and opaque. The Kubelka-Munk function is described for any wavelength as Equation (1) [22].

$$F(R) = \frac{(1 - R)^2}{2R} = \frac{k}{s} \quad (1)$$

where $F(R)$ denotes the Kubelka-Munk function and R is reflectance data. The k and s represent the molar absorption coefficient and scattering coefficient, respectively. With the purpose to estimate the optical bandgap

energy, E_g , of the direct bandgap of the PZN and rZN nanocomposites samples, the above equation was substituted into Tauc's relation and rewritten with the relationship as shown below [23]:

$$[F(R) \times hv]^2 = A(hv - E_g) \quad (2)$$

where hv represent photon energy, E_g denotes optical bandgap energy, and energy-independent constant is denoted as A. Figure 4a illustrates the modified Tauc's plot based on Kubelka-Munk function for bandgap energy approximation where the E_g values were produced at which the extrapolated linear region of $(F(R)*hv)^2$ versus incident photon energy curves intersects the incident photon energy axis, producing $(F(R)*hv)^2 = 0$. The average reflectance and E_g values are shown in Table 1.

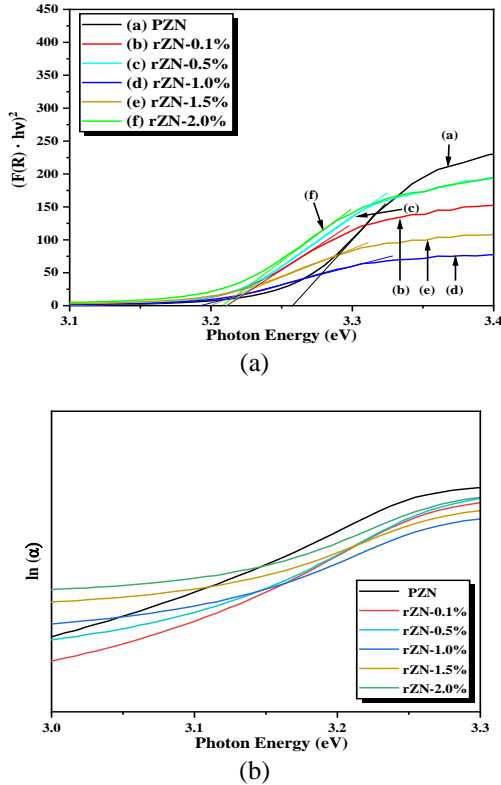


Figure 4: (a) Kubelka-Munk function plot of PZN and rZN nanocomposites, and (b) a plot for Urbach energy estimation

The E_g displayed a redshift with the expanding amount of rGO dosage in the nanocomposites. Initially, the bandgap energies decreased from 3.259 eV to 3.195 eV with 1.0 wt.% of rGO dosage level loaded into rZN nanocomposites. The E_g values slightly increased to 3.201 eV and 3.207 eV for 1.5 wt.% and 2.0 wt.% of rGO content, respectively. It would be reasonable to conclude that the presence of rGO has a certain effect on the electronic energy level of pristine ZnO. With a narrower bandgap, electrons may be transported more efficiently and rapidly from the sensing film to the electrode, resulting in decreased resistivity and improved conductivity, hence increasing the overall sensitivity of the humidity sensor [24]. Similar findings regarding narrower direct bandgap of rZN nanocomposites have been reported in previous research. Rodwihok et al. reported that the decrease in bandgap is driven by the optical bandgap shifting to a higher wavelength as the surface charge between ZnO and rGO increases [25]. Meanwhile, based on the finding by Dehghan et al. [26], suggested bandgap narrowing is attributed to synergistic interfacial interaction between the ZnO nanoparticles and rGO sheets. This statement is also consistent with the findings by Darvishi and associates [27]. Furthermore, the variation in bandgap energy could be due to particle aggregation and the formation of large clusters that induced the agglomeration of particles, as documented by previous researchers [28]-[29]. As a result, our findings, and observations of a redshift in the absorption edge of rZN nanocomposite samples against pristine ZN are supported.

Furthermore, structural defect estimation was studied using a variation of Urbach energy, E_u , as demonstrated in the given relation [30]:

$$\alpha = \alpha_0 \exp\left(\frac{h\nu}{E_u}\right) \quad (3)$$

where the absorption coefficient is denoted as α , the pre-exponential factor is represented as α_0 , $h\nu$ is known as photon energy, and Urbach energy denotes as E_u , which is the localized state width. The Urbach energy, which corresponds to the tail width of the localized states within the optical band gap, is related to the absorption coefficient at the lower essential edge energy region. The variation in E_u is related to band bending, which arises as a result of structural deficiency [31]. The linear component's reciprocal gradient of a plot of $\ln(\alpha)$ against photon energy, $h\nu$, was used to estimate Urbach energy as portrayed in Figure 4b.

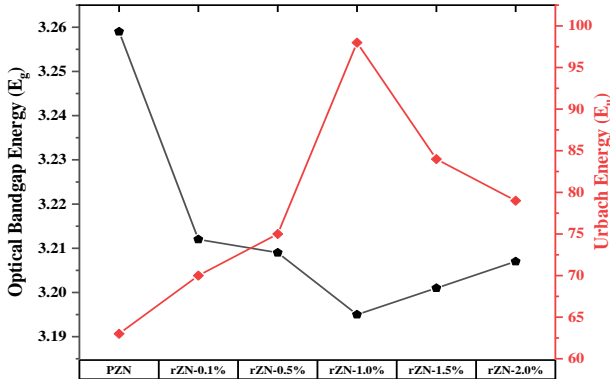


Figure 5: Bandgap and Urbach energy variation plot for PZN and rZN nanocomposites

Contrary to PZN, E_u values increased slightly as the rGO amount was introduced from 0.1 to 0.5 wt.% but significantly increased as rGO content increased from 1.0 wt.% to 2.0 wt.%, demonstrating the intensification of structural disorder. As depicted in Figure 5, the Urbach energy, E_u , varies inversely with the optical band gap energy, E_g . The fluctuation in Urbach tail energy suggests that the quantity of rGO content is important in the creation of defect levels in the ZnO lattice. Increased E_u value at a higher amount of rGO dosage levels was also reported by Rodwihok et. al [25] and Mangavati et. al [32]. The highest value of E_u was achieved at an rGO concentration of 1.0 wt.%, suggesting the prominent existence of defects/deficiency in rGO/ZnO synthesized at 1.0 wt.% rGO. Furthermore, as stated in Table 1, the increase in structural disorder may be the cause of the average reflectance significant decline.

Table 1: Average reflectance, and optical bandgap energy of PZN and rZN nanocomposites at different rGO dosage

Sample	rGO content (mg)	Average reflectance, R (%)	Optical bandgap energy, E_g (eV)	Urbach energy, E_u (meV)
PZN	0	78.31	3.259	63
rZN-0.1%	1	71.95	3.212	70
rZN-0.5%	5	59.59	3.209	75
rZN-1.0%	10	52.66	3.195	98
rZN-1.5%	15	41.94	3.201	84
rZN-2.0%	20	36.65	3.207	79

The PZN and rZN nanocomposites sensitivity towards humidity changes was examined via ESPEC-SH261 humidity and temperature chamber with Keithley 2400 Source Meter unit. During humidity sweeping analysis, a bias voltage (+ 5 V) was fed to the sensor with the temperature inside the chamber regulated at 25 °C to meet the temperature of the surroundings, during the measurement process. The measurement was performed for one complete cycle by stepping the RH from a baseline humidity (40 %RH) to a threshold humidity (90 %RH) and vice versa to examine the sensor response and recovery towards increasing and decreasing relative humidity. The sensitivity percentage, S, of the PZN and rZN nanocomposites was assessed using the accompanying relations, particularly concentrating on the ratio of resistance perturbations [33]:

$$\text{Sensitivity Percentage} = \left(\frac{R_{40\%} - R_X}{R_X} \right) \times 100 \quad (4)$$

where $R_{40\%}$ denotes the baseline humidity resistance and R_X is the resistance when humidity levels change. The sensitivity plots at 40 %RH, 50 %RH, 60 %RH, 70 %RH, 80 %RH and 90 %RH are presented in Figure 6 with the primary purpose of improving the sensitivity of the PZN by determining the optimal amount of rGO required is positively realized. The prevailing results observed on rZN-1.0% humidity sensor, which showed superior sensitivity compared to the other samples, were confirmed. This could be due to the lower energy bandgap reported earlier in conjunction with the highest Urbach energy recorded. According to Li [34], the incorporation of rGO increases the electrical conductivity behaviour of the rGO/ZnO composite, which enables high electrical propagation throughout the composite material, hence increasing the sensitivity of the composite as the relative humidity increases. It demonstrates that as the level of relative humidity rises, the resistance of the rZN nanocomposites falls roughly linear, implying that the humidity sensor based on rZN nanocomposite is sensitive to humidity compared to PZN. Moreover, this outcome might contribute by coordinated dispersion of ZN nanoparticles across rGO layers in humidity sensor based on rZN-1.0% nanocomposite, as well as the ideal synergetic reaction induced by ZN and rGO, which is in accordance with our FESEM analysis.

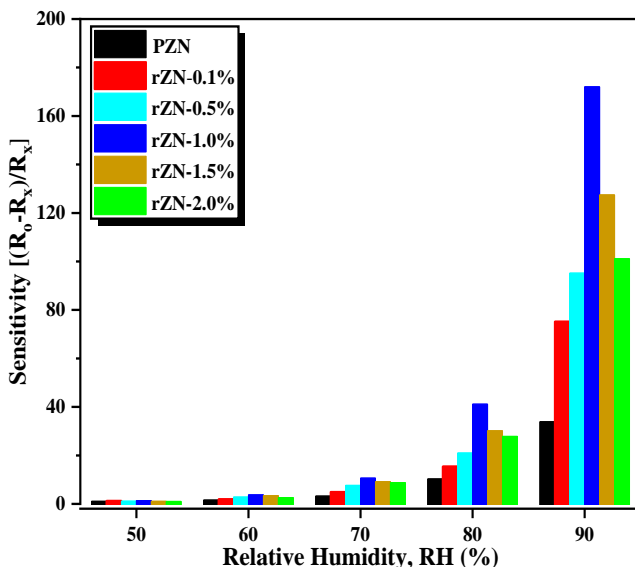


Figure 6: Sensitivity profiles of PZN and rZN nanocomposite-based humidity sensors at different humidity levels with varying weight percentages of rGO dosage at 25 °C

The sensitivity trajectory in Figure 7 shows a substantial enhancement in sensitivity driven by optimal rGO dosage at multiple measurement attempts. The addition of rGO boosted the sensitivity thresholds from 3500% for PZN-based humidity sensor to 17300% for rZN-1.0% based humidity sensor. The standard deviation for rZN-1.0 was less than 2%, showing that the sensitivity was repeatable from measurement to measurement. However, when the amount of rGO injected was higher than 1.0 wt.%, the sensitivity of the sensors was significantly diminished. The findings of this study are contrasted with other relevant publications by other researchers [35]–[38]. According to our literature, we concluded that the performance of the humidity sensor attained in our investigation is equitable to or better than those found in prior reports.

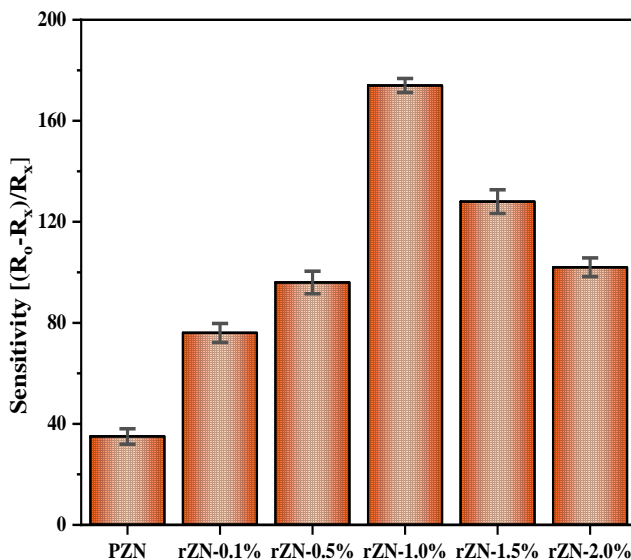


Figure 7: The variation in sensitivity of humidity sensors based on PZN and rZN nanocomposite. The computed mean values and error bars are displayed from the datasets of five observations

Figure 8 depicts the humidity response profiles of the rZN-1.0% based humidity sensor at various operational temperatures of 25 °C, 45 °C, 65 °C, and 85 °C. The results reveal that the humidity response curve patterns at varying temperatures are nearly comparable with a varied current rate. At higher temperatures, the humidity response at exhibits greater current responsiveness than those occurring at minimal operational temperatures. At tested temperatures of 25 °C, 45 °C, 65 °C, and 85 °C, the sensitivity stats were computed to be 17300%, 13000%, 11500%, and 10500%, respectively. The decreased sensitivity as the temperature rises is possibly attributed to the reduction in water molecules and oxygen molecules diffusion depth [39]. As the sensitivity is noticeably reduced at the high operating temperature, on the other hand, the humidity response signal amplifies, which is observed during the measurement procedure the current value increased substantially [40].

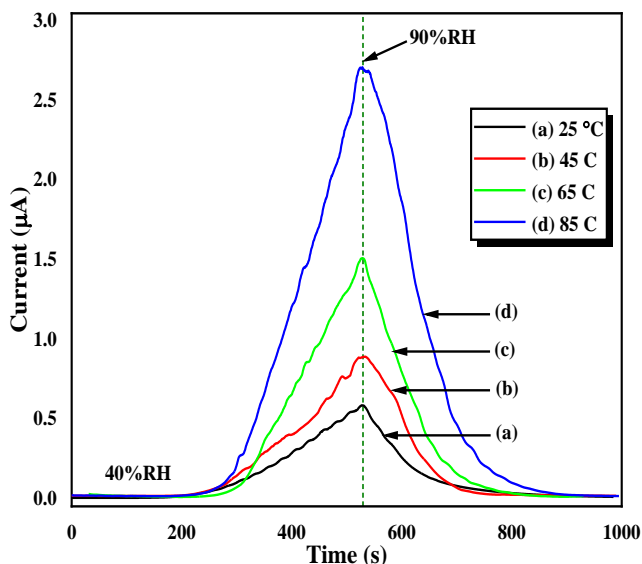


Figure 8: The rZN-1.0% humidity response profile at various operation temperatures

Conclusion

In this work, the facile ultrasonicated solution immersion approach was used to successfully synthesize ZN. Moreover, the PZN and rZN nanocomposites were successfully deposited on a cellulose substrate by employing the brush printing technique at different rGO concentration doses. The structural, morphological and optical characteristics of the sensing membrane have been explored. XRD investigation corroborated the polycrystalline arrangement of solid with crystalline hexagonal wurtzite of the PZN and rZN nanocomposite structure. The rGO adhered to the surface of the ZN, with no impurity-related peaks identified. Based on FESEM investigation, ZN nanoparticles of varied sizes were uniformly distributed, adhered to, and arbitrarily positioned onto the cellulose strands. In comparison to PZN, the composite with rGO dosage had less particle agglomeration and aggregation. All rZN nanocomposites possess a porosity structure, which is estimated to continue providing active sites for water molecule adsorption. The band gap determined from DRS spectra for PZN is 3.259 eV and observed to decrease to 3.212 eV with rGO content of 0.1 wt.% and reaches a minimum of 3.195 eV with rGO content of 1.0 wt.%. The existent correlations among the Zn, C, and O atoms are the fundamental sources of the band gap reduction. The optical band gap and

Urbach energy were discovered to be inversely proportional to the amount of rGO inserted. Moreover, as the rGO amount increased, the average reflectance in the visible region decreased substantially. When the rGO concentration was increased, the calculated Urbach energy of the rZn nanocomposites soared indicating that the formation of defects and disorders is also accountable for the shrinking of the band gap. Furthermore, the enrichment of local disorders driven by the extrinsic element is associated with the increment of E_u . In terms of sensitivity, rZn nanocomposites-based humidity sensors surpassed PZn-based humidity sensor, with 1.0 wt.% rGO dosage exhibiting the maximum sensitivity towards humidity. The humidity response exhibits an increased current value at high operational temperatures, but a reduced sensitivity value was recorded as an impact from the baseline current value (40 %RH). Morphological, optical and humidity sensing analysis results indicate that the rZn nanocomposite material is advantageous for inexpensive and economical flexible humidity sensing applications. and manipulating the amount of rGO amount inserted in metal oxide is significantly important.

Acknowledgement

The authors would like to express their gratitude to the Kementerian Pengajian Tinggi, Pusat Pengajian Kejuruteraan Elektrik, Kolej Kejuruteraan, UiTM Shah Alam, and Fakulti Teknologi Kejuruteraan Elektrik dan Elektronik (FTKEE), UTeM. This research is funded by the Fundamental Research Grant Scheme (FRGS) (FRGS/1/2022/TK07/UITM/02/7) from Ministry of Higher Education Malaysia.

References

- [1] N. Parimon *et al.*, “Annealing temperature dependency of structural, optical and electrical characteristics of manganese-doped nickel oxide nanosheet array films for humidity sensing applications,” *Nanomater. Nanotechnol.*, vol. 11, pp. 1–13, 2021.
- [2] M. Z. Musa *et al.*, “Fabrication and structural properties of flower-like TiO₂ nanorod array films grown on glass substrate without FTO layer,” *Mater. Lett.*, vol. 273, p. 127902, 2020.
- [3] M. Mohamed Zahidi *et al.*, “Evaluating Different TiO₂ Nanoflower-Based Composites for Humidity Detection,” *Sensors*, vol. 22, no. 15, p. 5794, Aug. 2022.
- [4] M. A. Najeeb, Z. Ahmad, and R. A. Shakoor, “Organic Thin-Film Capacitive and Resistive Humidity Sensors: A Focus Review,” *Adv.*

- Mater. Interfaces*, vol. 5, no. 21, pp. 1–19, 2018.
- [5] Yu, Zhang, Zhang, and Li, “Effects of pH on High-Performance ZnO Resistive Humidity Sensors Using One-Step Synthesis,” *Sensors*, vol. 19, no. 23, p. 5267, Nov. 2019.
- [6] Y. B. Hahn, “Zinc oxide nanostructures and their applications,” *Korean J. Chem. Eng.*, vol. 28, no. 9, pp. 1797–1813, 2011.
- [7] D. Zhang, J. Liu, and B. Xia, “Layer-by-Layer Self-Assembly of Zinc Oxide/Graphene Oxide Hybrid Toward Ultrasensitive Humidity Sensing,” *IEEE Electron Device Lett.*, vol. 37, no. 7, pp. 916–919, 2016.
- [8] S. Narasimman, U. Dinesh, L. Balakrishnan, S. R. Meher, R. Sivacoumar, and Z. C. Alex, “A comparative study on structural, optical and humidity sensing characteristics of ZnO, SnO₂ and ZnO:SnO₂ nanocomposite,” *Sens. Lett.*, vol. 15, no. 5, pp. 440–447, 2017.
- [9] R. Tarcan, O. Todor-Boer, I. Petrovai, C. Leordean, S. Astilean, and I. Botiz, “Reduced graphene oxide today,” *J. Mater. Chem. C*, vol. 8, no. 4, pp. 1198–1224, 2020.
- [10] H. Yan, Z. Chen, L. Zeng, Z. Wang, G. Zheng, and R. Zhou, “The effect of rgo-doping on the performance of SnO₂/rGO flexible humidity sensor,” *Nanomaterials*, vol. 11, no. 12, 2021.
- [11] M. Morsy, M. M. Mokhtar, S. H. Ismail, G. G. Mohamed, and M. Ibrahim, “Humidity Sensing Behaviour of Lyophilized rGO/Fe₂O₃ Nanocomposite,” *J. Inorg. Organomet. Polym. Mater.*, vol. 30, no. 10, pp. 4180–4190, 2020.
- [12] F. Wang *et al.*, “Flexible wearable graphene/alginate composite non-woven fabric temperature sensor with high sensitivity and anti-interference,” *Cellulose*, vol. 7, 2019.
- [13] A. S. R. A. Subki *et al.*, “Effects of varying the amount of reduced graphene oxide loading on the humidity sensing performance of zinc oxide/reduced graphene oxide nanocomposites on cellulose filter paper,” *J. Alloys Compd.*, vol. 926, p. 166728, 2022.
- [14] S. Chaudhary *et al.*, “Reduced Graphene Oxide/ZnO Nanorods Nanocomposite: Structural, Electrical and Electrochemical Properties,” *J. Inorg. Organomet. Polym. Mater.*, vol. 29, no. 6, pp. 2282–2290, 2019.
- [15] K. Chaudhary *et al.*, “Graphene oxide and reduced graphene oxide supported ZnO nanochips for removal of basic dyes from the industrial effluents,” *Fullerenes Nanotub. Carbon Nanostructures*, vol. 29, no. 11, pp. 915–928, 2021.
- [16] R. Ponnusamy *et al.*, “Experimental and density functional theory investigations of catechol sensing properties of ZnO/RGO nanocomposites,” *Appl. Surf. Sci.*, vol. 495, no. September 2018, p. 143588, 2019.
- [17] S. H. Ferreira *et al.*, “Uv-responsive screen-printed porous zno nanostructures on office paper for sustainable and foldable electronics,”

- Chemosensors*, vol. 9, no. 8, 2021.
- [18] M. Salem, S. Akir, I. Massoudi, Y. Litaïem, M. Gaidi, and K. Khirouni, "Photoelectrochemical and optical properties tuning of graphene-ZnO nanocomposites," *J. Alloys Compd.*, vol. 767, pp. 982–987, 2018.
- [19] Z. Ren *et al.*, "Cr(VI) reduction in presence of ZnS/RGO photocatalyst under full solar spectrum radiation from UV/vis to near-infrared light," *Catal. Today*, vol. 315, no. October 2017, pp. 46–51, 2018.
- [20] B. Weng, M. Q. Yang, N. Zhang, and Y. J. Xu, "Toward the enhanced photoactivity and photostability of ZnO nanospheres via intimate surface coating with reduced graphene oxide," *J. Mater. Chem. A*, vol. 2, no. 24, pp. 9380–9389, 2014.
- [21] Y. Feng, N. Feng, Y. Wei, and G. Zhang, "An in situ gelatin-assisted hydrothermal synthesis of ZnO-reduced graphene oxide composites with enhanced photocatalytic performance under ultraviolet and visible light," *RSC Adv.*, vol. 4, no. 16, pp. 7933–7943, 2014.
- [22] E. A. Araújo *et al.*, "Synthesis, growth mechanism, optical properties and catalytic activity of ZnO microcrystals obtained via hydrothermal processing," *RSC Adv.*, vol. 7, no. 39, pp. 24263–24281, 2017.
- [23] L. F. Koao *et al.*, "Effects of octadecylamine molar concentration on the structure, morphology and optical properties of ZnO nanostructure prepared by homogeneous precipitation method," *J. Lumin.*, vol. 200, no. April, pp. 206–215, 2018.
- [24] S. A. M. Chachuli *et al.*, "Effects of MWCNTs/graphene nanoflakes/MXene addition to TiO₂ thick film on hydrogen gas sensing," *J. Alloys Compd.*, vol. 882, 2021.
- [25] C. Rodwihok, D. Wongratanaphisan, Y. L. T. Ngo, M. Khandelwal, S. H. Hur, and J. S. Chung, "Effect of GO additive in ZnO/rGO nanocomposites with enhanced photosensitivity and photocatalytic activity," *Nanomaterials*, vol. 9, no. 10, 2019.
- [26] S. Dehghan, M. Tahergorabi, S. Norzaee, E. Boorboor Azimi, M. Hasham Firooz, and Y. Dadban Shahamat, "Preparation and photocatalytic performance of reduced graphene oxide/ ZnO nanocatalyst for degradation of metalaxyl from aqueous solution: effect of operational parameters, mineralisation and toxicity bioassay," *Int. J. Environ. Anal. Chem.*, vol. 00, no. 00, pp. 1–23, 2020.
- [27] M. Darvishi, F. Jamali-Paghaleh, M. Jamali-Paghaleh, and J. Seyed-Yazdi, "Facile synthesis of ZnO/rGO hybrid by microwave irradiation method with improved photoactivity," *Surfaces and Interfaces*, vol. 9, no. April, pp. 167–172, 2017.
- [28] D. Dastan, S. L. Panahi, and N. B. Chaure, "Characterization of titania thin films grown by dip-coating technique," *J. Mater. Sci. Mater. Electron.*, vol. 27, no. 12, pp. 12291–12296, 2016.
- [29] N. Parimon *et al.*, "Fabrication, structural, optical, electrical, and humidity sensing characteristics of hierarchical NiO nanosheet/nanoball-

- flower-like structure films,” *J. Mater. Sci. Mater. Electron.*, vol. 31, no. 14, pp. 11673–11687, 2020.
- [30] A. S. Ismail *et al.*, “Modulation of Sn concentration in ZnO nanorod array: intensification on the conductivity and humidity sensing properties,” *J. Mater. Sci. Mater. Electron.*, vol. 29, no. 14, pp. 12076–12088, 2018.
- [31] M. F. Malek *et al.*, “Metamorphosis of strain/stress on optical band gap energy of ZAO thin films via manipulation of thermal annealing process,” *J. Lumin.*, vol. 160, pp. 165–175, 2015.
- [32] S. Mangavati *et al.*, “Defects and band gap shrinkage in ZnO/rGO composite nano-pebbles prepared by solid–state reaction,” *Diam. Relat. Mater.*, vol. 123, no. February, p. 108886, 2022.
- [33] V. Verma, N. K. Pandey, P. Gupta, K. Singh, and P. Singh, “Humidity sensing enhancement and structural evolution of tungsten doped ZnO nanosensors fabricated through co-precipitation synthesis,” *Phys. B Condens. Matter*, vol. 619, no. March, p. 413224, 2021.
- [34] X. Li, Z. Wang, Y. Qiu, Q. Pan, and P. Hu, “3D graphene/ZnO nanorods composite networks as supercapacitor electrodes,” *J. Alloys Compd.*, vol. 620, pp. 31–37, 2015.
- [35] M. Morsy, M. Ibrahim, Z. Yuan, and F. Meng, “Graphene Foam Decorated with ZnO as a Humidity Sensor,” *IEEE Sens. J.*, vol. 20, no. 4, pp. 1721–1729, 2020.
- [36] D. Zhang *et al.*, “Humidity-sensing properties of hierarchical ZnO/MWCNTs/ZnO nanocomposite film sensor based on electrostatic layer-by-layer self-assembly,” *J. Mater. Sci. Mater. Electron.*, vol. 27, no. 3, pp. 2481–2487, 2016.
- [37] C. Chen, X. Wang, M. Li, Y. Fan, and R. Sun, “Humidity sensor based on reduced graphene oxide/lignosulfonate composite thin-film,” *Sensors Actuators, B Chem.*, vol. 255, pp. 1569–1576, 2018.
- [38] Y. Chen *et al.*, “Plasma assisted molecular beam epitaxy of ZnO on c-plane sapphire: Growth and characterization,” *J. Appl. Phys.*, vol. 84, no. 7, pp. 3912–3918, 1998.
- [39] M. H. Mamat *et al.*, “Heterojunction of SnO₂ nanosheet/arrayed ZnO nanorods for humidity sensing,” *Mater. Chem. Phys.*, vol. 288, p. 126436, 2022.
- [40] J. Liu *et al.*, “Highly sensitive and low detection limit of ethanol gas sensor based on hollow ZnO/SnO₂ spheres composite material,” *Sensors Actuators, B Chem.*, vol. 245, pp. 551–559, 2017.